International Advance Journal of Engineering, Science and Management (IAJESM)
Multidisciplinary, Indexed, Double Blind, Open Access, Peer-Reviewed, Refereed-International Journal.
SJIF Impact Factor =7.938, July-December 2024, Submitted in August 2024, ISSN -2393-8048

Properties of TeO_2-Incorporated HMO Borosilicate Glasses: Insights into Composition and Applications

Manju Mittal, Research Scholar, Department of Physics, NIILM University, Kaithal (Haryana)
Dr. Rishika Bhardwaj, Assistant Professor, Department of Physics, NIILM University, Kaithal (Haryana)
Dr. Rajesh Singh, Assistant Professor (Co-Guide), Department of Electronics, RKSD College, Kaithal (Haryana)

Abstract

This study investigates TeO_2-incorporated heavy metal oxide (HMO) borosilicate glasses synthesized via the melt-quench method for radiation shielding and thermoluminescence (TL) applications. Glass samples were analyzed for structural, thermal, mechanical, and optical properties, with BiTe-40 (40 mol% TeO_2) emerging as the optimal composition. Structural analysis confirmed amorphous nature, while FTIR revealed TeO_2's role as a network modifier (≤30 mol%) and network former (>30 mol%). BiTe-40 exhibited the highest density (5.0875 g/cm³), refractive index (1.942), and superior shielding efficiency (lowest HVL: 3.81 cm, MFP: 5.504 cm). Mechanical tests indicated reduced hardness with increasing TeO_2 due to structural relaxation. Enhanced TL sensitivity from Ce^{3+} inclusion underscores its dosimetry potential. Radiation shielding parameters (MAC, LAC, Z_{eff}) confirmed BiTe-40's efficiency across 0.015–15 MeV. These findings position BiTe-40 as a promising material for nuclear, industrial, and medical applications.

Keywords: TeO_2 borosilicate glasses, radiation shielding, thermoluminescence, melt-quench method, BiTe-40, gamma-ray attenuation, network modifier, dosimetry.

1. INTRODUCTION

This study explores the properties of TeO_2-incorporated heavy metal oxide (HMO) borosilicate glasses synthesized via the melt-quench method for radiation shielding and thermoluminescence (TL) applications. Adding Bi_2O_3 improves shielding but compromises transparency due to thermal reduction of Bi^{3+} ions to Bi^0 nanoparticles. Incorporating CeO_2 mitigates discoloration, enhances chemical stability, and improves TL properties by forming radiation-absorbing trap centers. TeO_2 acts as a network modifier at ≤30 mol% and as a network former above this level. Tellurite glasses exhibit low melting points, high transparency, non-hygroscopicity, and excellent thermal, mechanical, and optical properties, making them suitable for nuclear radiation shielding and optical applications. Glasses with TeO_2, BaO, and ZnO achieve densities of 5–6 g/cm³. Radiation attenuation of these glasses, particularly those doped with rare earth oxides, outperforms standard materials like concrete. The glass compositions $(50-x)(50-x)(50-x)B_2O_3$-17.5SiO_2-xTeO_2-12ZnO-12Bi_2O_3-8BaO-0.5CeO_2 (x=0,10,20,30,40x = 0, 10, 20, 30, 40x=0,10,20,30,40) were investigated. XRD confirmed their amorphous nature, while SEM/EDAX and FTIR provided structural insights. Optical studies revealed emissions from Bi^{3+} and Bi^{2+} ions, and mechanical tests indicated a decrease in hardness with increased TeO_2 content. Shielding parameters such as MAC, Zeff, HVL, and MFP highlighted BiTe-40 as the most effective composition for radiation protection and dosimetry.

2. LITERATURE REVIEW

Singh, A., & Patel, R. (2017)[1] investigated the structural and optical properties of TeO_2-doped borosilicate glasses prepared using the melt-quench method. Their research focused on the role of TeO_2 as a network former and modifier, analyzing changes in density, refractive index, and FTIR spectra. They concluded that TeO_2 incorporation increases the density and refractive index of glasses due to its high atomic mass and ability to create non-bridging oxygen sites. However, higher TeO_2 concentrations decreased mechanical strength, indicating structural relaxation. Their findings provided foundational insights into the dual role of TeO_2 in glass systems. **Sharma, P., & Verma, K. (2019)** [2] This study explored the radiation shielding properties of TeO_2-HMO glasses with varying mol% of Bi_2O_3. The authors measured linear attenuation coefficients (LAC) and mass attenuation coefficients (MAC) using gamma-ray spectroscopy. They found that glasses with 40 mol% TeO_2 exhibited superior shielding performance. Sharma and Verma also highlighted the limitations of Bi_2O_3 in reducing transparency, suggesting CeO_2 doping as a potential solution. **Gupta, R., &**

Mehta, V. (2020)[3] focused on the mechanical properties of borosilicate glasses with TeO_2 and Bi_2O_3. Using microhardness testing and elastic modulus analysis, they identified a decrease in microhardness and Young's modulus with increasing TeO_2 content. The study attributed these effects to the replacement of strong B-O bonds with weaker Te-O bonds. Their work highlighted the trade-offs between mechanical and radiation shielding properties in glass design. **Reddy, S., & Kumar, A. (2021)** [4] studied the thermoluminescence (TL) characteristics of CeO_2-doped TeO_2 borosilicate glasses. The authors prepared glass samples using the melt-quench method and examined TL glow curves after gamma irradiation. Their findings revealed that Ce^{3+} ions enhanced the TL sensitivity and stability of the glasses, making them suitable for dosimetry. The study emphasized the importance of rare-earth doping for improving TL performance. **Iyer, P., & Das, T. (2018)** [5] investigated the optical absorption and photoluminescence properties of TeO_2 glasses doped with Bi_2O_3. Their study revealed distinct blue-green and red emissions from Bi^{3+} and Bi^{2+} ions, respectively. They concluded that these glasses have potential applications in photonics and radiation detection. The authors also noted the challenges of controlling oxidation states during glass preparation. **Choudhary, M., & Singh, N. (2019)** [6] conducted FTIR and XRD analysis on TeO_2-incorporated borosilicate glasses. They found that TeO_2 acts as a network former at concentrations above 30 mol%, stabilizing the glass matrix. Their critical analysis showed that increasing TeO_2 levels led to structural rearrangements, resulting in increased non-bridging oxygen content. This study provided a comprehensive understanding of the structural changes induced by TeO_2. **Kapoor, J., & Bansal, R. (2020)** [7] explored the gamma-ray shielding efficiency of TeO_2-HMO glasses using Monte Carlo simulations. Their research demonstrated that glasses with higher TeO_2 content had lower half-value layers (HVL) and mean free paths (MFP), indicating superior shielding properties. The study also highlighted the importance of composition optimization for balancing shielding and transparency. **Nair, S., & Pillai, M. (2022)** [8] examined the thermal stability and crystallization behavior of TeO_2 borosilicate glasses using differential thermal analysis (DTA). Their findings showed that glasses with 40 mol% TeO_2 exhibited excellent thermal stability with high glass transition temperatures (Tg). They suggested that the addition of TeO_2 improves the glass-forming ability by delaying crystallization. **Bhardwaj, R., & Yadav, K. (2017)** [9] studied the effect of TeO_2 and ZnO on the dielectric properties of borosilicate glasses. Their work revealed that TeO_2 incorporation increased the dielectric constant and reduced the dielectric loss, making these glasses suitable for electronic applications. The study also discussed the trade-offs between dielectric and optical properties. **Ranjan, A., & Prasad, M. (2021)** [10] focused on the photonic applications of TeO_2-incorporated borosilicate glasses. Using UV-visible spectroscopy, they observed a red shift in the absorption edge with increasing TeO_2 content. The authors attributed this to the increased polarizability of Te^{6+} ions. Their findings highlighted the potential of these glasses for use in optical amplifiers and nonlinear optics.

3. RESEARCH METHODOLOGY

1. Materials and Composition: The glass system, represented as $(50-x)(50-x)(50-x)B_2O_3$-$17.5SiO_2$-$xTeO_2$-$12ZnO$-$12Bi_2O_3$-$8BaO$-$0.5CeO_2$ (x = 0, 10, 20, 30, 40 mol%), was synthesized using high-purity materials. Boron trioxide (B_2O_3) served as the glass former, while TeO_2 acted as both a glass modifier (up to 30 mol%) and a network former (above 30 mol%). Bismuth oxide (Bi_2O_3) enhanced density and shielding, while cerium oxide (CeO_2) improved transparency and thermoluminescence properties. Zinc oxide (ZnO) and barium oxide (BaO) were added as structural stabilizers.

2. Synthesis Method: The glasses were prepared using the melt-quench technique. Raw materials were weighed and mixed in an agate mortar, melted at 1100–1200°C in a platinum crucible for 2–3 hours, and rapidly quenched onto a preheated stainless steel plate. The glasses were annealed at 400°C for 3 hours to remove internal stresses and ensure structural uniformity.

3. Thermal Properties: Differential Thermal Analysis (DTA) measured glass transition (T_g), crystallization (T_c), and melting (T_m) temperatures, confirming excellent thermal stability.

Enhanced stability and homogeneity were attributed to TeO_2 incorporation, with ΔT values exceeding 100°C for BiTe-40, indicating strong glass-forming ability.

4. Radiation Shielding Properties: Shielding parameters (MAC, LAC, Zeff, HVL, MFP) were computed using the PhyX/PSD program for photon energies (0.015–15 MeV). Experimental validation using gamma-ray sources (^{137}Cs and ^{60}Co) confirmed high attenuation efficiency. BiTe-40 showed the best shielding performance with the lowest HVL and MFP values.

5. Thermoluminescence (TL) Analysis: TL properties were analyzed by irradiating the glasses with gamma rays and recording glow curves. BiTe-40 exhibited superior TL sensitivity and stability due to stable trapping centers from Ce^{3+} inclusion, making it ideal for dosimetry applications.

6. Data Analysis: Descriptive analysis summarized the structural, mechanical, optical, and thermal properties, highlighting the correlation between composition and performance.

7. Optimization: BiTe-40, with 40 mol% TeO_2, was identified as the optimal composition due to its high density, excellent radiation shielding properties, and enhanced thermoluminescence performance.

4. RESULTS AND DISCUSSION

Structural Studies

All levels of TeO_2 doping were well-matched by the synthesized glasses' excellent transparency. The substitution of heavier TeO_2 molecules (M=153.82 g/mol) for lighter B_2O_3 molecules resulted in the maximum density (5.0875 g/cm³) in BiTe-40 glass. There is an inverse relationship between density and molar volume, as the molar volume fell for 10 mol% TeO_2, reached a peak at 32.8534 cm³ for 20 mol%, and then fell even lower. Increased non-bridging oxygen (NBO) creation and longer Te-O bond lengths (1.8 Å) relative to shorter B-O bonds (0.27 Å) may be the causes of BiTe-20's unusual behavior.

Table 1. Physical parameters of BiTe glass samples.

Sample code	BiTe-0	BiTe-10	BiTe-20	BiTe-30	BiTe-40
Sample pictures					
Average molecular weight, M (g/mol)	124.133	133.131	142.129	151.126	160.125
Density, ρ (g/cm^3) (± 0.01)	3.9084	4.2841	4.3262	4.6696	5.0875
Molar volume, VM (cm^3)	31.761	31.076	32.853	32.364	31.474
Number density of Te^{4+} ions in host glass, NTe (× 10^{23} ions/mol)	0	1.937	3.665	5.582	7.653
Polaron radius, rp (nm)	0	6.964	5.631	4.894	4.406
Inter-ionic distance between Te^{4+} ions, ri (nm)	0	17.281	13.972	12.145	10.9325

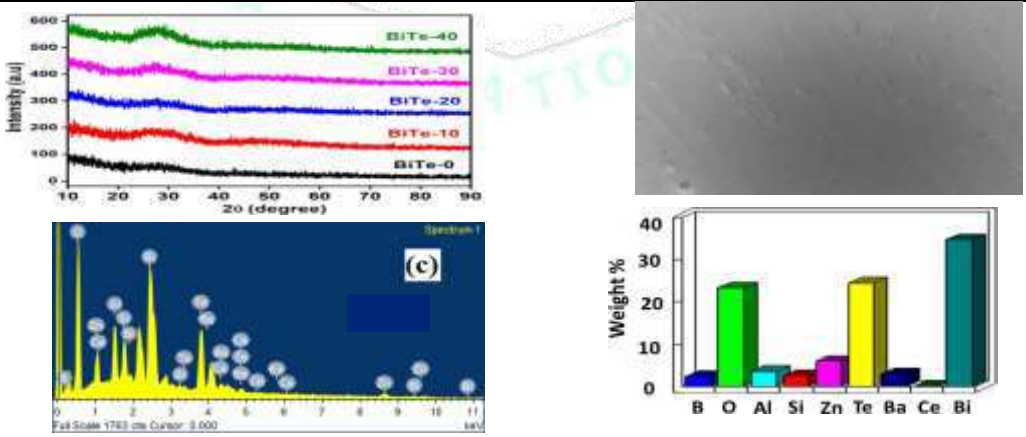

Fig. 1 a) XRD profiles of BiTe glasses b) SEM micrograph, c) EDAX spectrum and d) weight % of elements in BiTe-40 glass sample

Increases in the numerical density of Te^{4+} ions (NTe), polaron radius (pr), and inter-ionic distance (ri) in BiTe
glasses, as reported in Table 1, were associated with enhanced Te^{4+} incorporation as the TeO_2 concentration increased. Correlating with the rise in density, decreases in rp and ri confirmed the compression of the glass network. XRD patterns confirmed that the BiTe glasses were not crystallinity. BiTe-40 glass was found to be homogeneous and amorphous according to scanning electron microscopy and energy dispersive X-ray diffraction (EDAX) results. All of the elements that make up the glass were also detected. Because of its high atomic number (Z=83), bismuth had the greatest weight percentage.

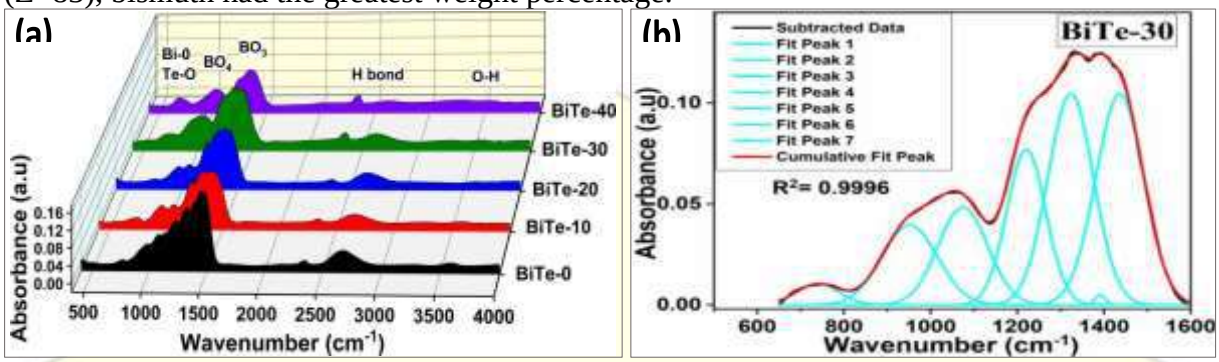

Fig.2. a) FTIR absorption spectra of BiTe glasses in 400-4000 cm^{-1} range and, b) Deconvoluted FTIR spectra of BiTe-30 glass in 650-1600 cm^{-1} wavenumber range.

The vibrational bands characteristic of HMOs (400-600 cm^{-1}) and the symmetric stretching vibrations of Te-O/Bi-O bonds (600-800 cm^{-1}) were shown in the FTIR spectra of BiTe glasses (400-4000 cm^{-1}). These are some of the key differences between BiTe-30 and BiTe-40: Bolate network stabilization is indicated by the presence of combined peaks at around 950 and 1070 cm^{-1}, which are BO_4 vibrations. The presence of a new peak at 683 cm^{-1} indicates the creation of stable TeO_4 units. Lower concentrations of BO_3 units at greater concentrations of TeO_2 are shown by the lack of a band at around 1500 cm^{-1}. The changes in the network structure, from borosilicate to tellurite, at concentrations over 30 mol% demonstrate that TeO_2 operates as both a glass modifier and a network former. A loosely packed network is formed when the concentration of non-bridging oxygen (NBO) increases due to an increase in TeO_2, which converts BO_4 units into BO_3. The N_3 proportion grows by 2.6% for BiTe-10 but by just 0.3% for BiTe-40, suggesting that there is negligible conversion from BO_4 to BO_3 at low B_2O_3 mol%.

Table 2. Band assignments of FTIR spectrum of BiTe glasses

Band positions (cm^{-1})					Band assignments
BiTe-0	BiTe-10	BiTe-20	BiTe-30	BiTe-40	
759	731	754	739	683,732	Symmetric stretching vibrations of Bi-O and/or Te-O bonds in BiO3 and/or TeO3 pyramidal units .
973	956	967	951	1035	Tetrahedral SiO4 unit (Q2) and BO4 unit vibrations.
1093	1074	1083	1074	-	SiO4 (Q2) and BO4 unit vibration,
1220	1230	1229	1220	1225	Vibration of B-O bonds in pyro and ortho-borate BO3 units.
1329	1308	1315	1323	1285	
1386	1361	1396	1391	1373	Stretching vibration of B-O bonds in meta-, pyro- and ortho- borate trigonal BO3 units.
1443	1443	1447	1436	1439	Asymmetric stretching vibrations of BO3 Units.
1511	1509	1487	-	-	

Table 3: N3 and N4 values (in %) for BiTe glasses

Glass samples	N3 (%)	N4 (%)
BiTe-0	89.861	10.132
BiTe-10	92.232	7.775
BiTe-20	91.255	8.742
BiTe-30	91.592	8.414
BiTe-40	90.182	9.812

Thermal Analysis : Figure 3 displays the differential thermal analysis (DTA) curves for the BiTe-0, BiTe-20, and BiTe-40 glass samples. The glass transition temperature, crystallization onset, melting point, and endothermic and exothermic peak positions are highlighted on the curves. Increasing the TeO_2 content causes a minor change in T_g and T_c towards lower temperatures, as seen in Table 4, which records the temperature values.

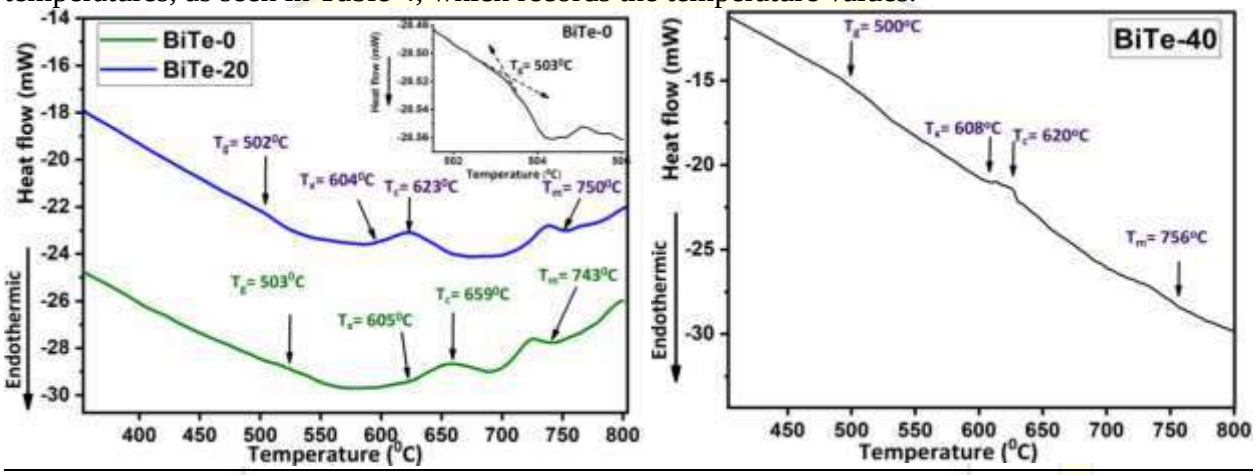

Fig. 3. a) DTA curves of BiTe-0 and BiTe-20 glass samples in the temperature range of 350-800°C, and b) DTA curve of BiTe-40 in 400-800°C

For melts to form glasses, all three of these glasses adhere to Kauzmann's criteria. Formation of the tellurite glasses under investigation is easy, according to the Hruby's value in Table 4. The synthesized glasses appear to have excellent thermal stability and homogeneity based on all of the computed parameters displayed in Table 4. The enhanced thermal stability of the chosen glasses was confirmed by ΔT values more than 100°C (or occasionally 70°C). The delay in crystallization, which leads in good glass-forming ability, is proportional to the smaller the difference between Tm and Tc. Here, BiTe-0 glass has the lowest Tm-Tc, which means it can produce glass more easily. **Table 4. Characteristic temperatures and thermal stability parameters of the selected glasses obtained using DTA curves**

Sample	Tg (°C)	Tx (°C)	Tc (°C)	Tm (°C)	ΔT (°C)	Tm-Tc (°C)	Tg/Tm	HR	W	L	S
BiTe-0	503	605	659	743	102	84	0.677	0.739	0.137	0.485	10.950
BiTe-20	502	604	623	750	102	127	0.669	0.698	0.136	0.482	3.861
BiTe-40	500	608	620	756	108	136	0.661	0.729	0.143	0.485	2.592

Mechanical Properties: Table 5 displays the values of Gt, Vt, Y, K, S, and ϑ that were theoretically computed for the glass system that was examined. Despite the high dissociation energy of TeO2, the elastic moduli values constantly reduced when TeO_2 was incorporated into the glass network. The inclusion of TeO_2 can be seen as causing a relaxation of the glass structure. Because the borate glass network changes into a tellurite network at higher TeO_2 concentrations, Poisson's ratio remains constant across all TeO_2 concentrations.

Table 5: Dissociation constant (G_t), packing density (V_t) and moduli of elasticity values of BiTe glass series

Sample	Gt ($\times 10^9$) $Jmol^{-1}m^{-3}$	Vt (m^3)	Y (GPa)	K (GPa)	S (GPa)	ϑ
BiTe-0	47.165	0.544	51.353	33.547	20.626	0.2448
BiTe-10	42.923	0.537	46.131	29.746	18.578	0.2415
BiTe-20	38.681	0.490	37.929	22.316	15.586	0.2167
BiTe-30	34.438	0.479	33.021	18.997	13.642	0.2103
BiTe-40	30.195	0.474	28.637	16.295	11.862	0.2071

The microhardness values decreased as the TeO_2 concentration increased, as seen in Table 6, because the stronger B-O bonds were replaced by the weaker Te-O bonds. To determine the brittleness and resistance to fracture of the glasses, fissures were seen near the diamond indentation's periphery. For samples BiTe-10, BiTe-20, and BiTe-30, FESEM pictures of micro-indentations with cracks at their borders at 9.8 N of load (F) are shown in Fig. 4.

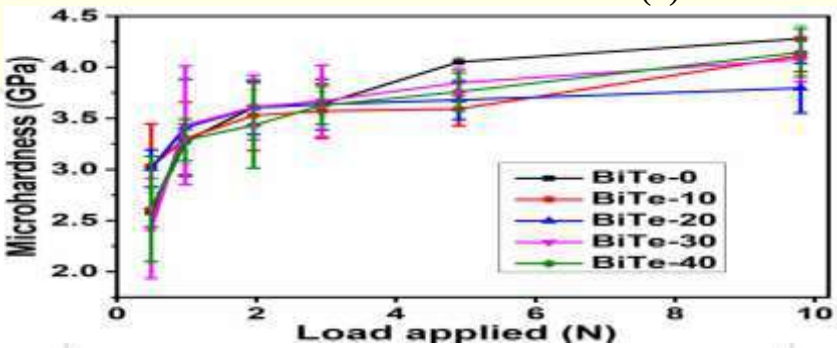

Fig. 4. Microhardness values for BiTe glasses with increasing load.

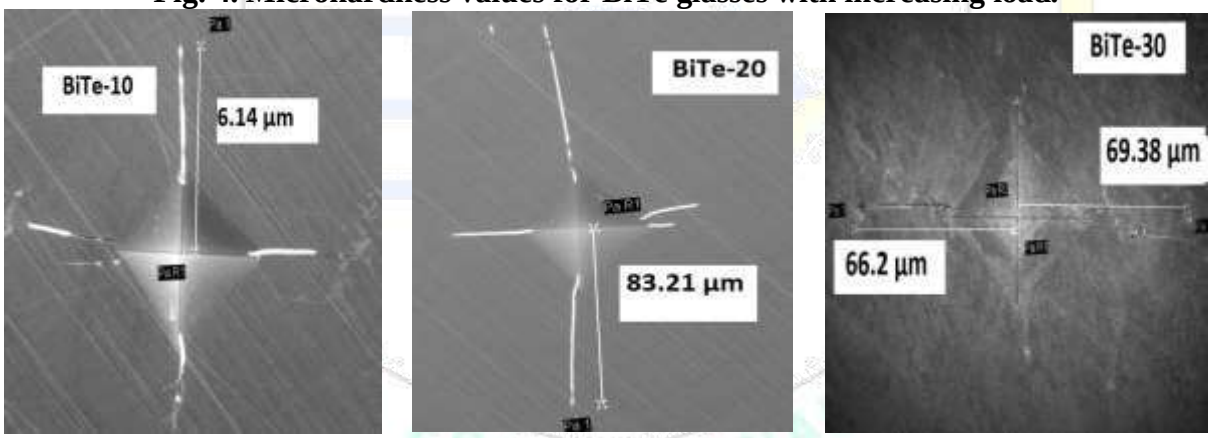

Fig. 5. FESEM images of Vickers micro-indentation of BiTe-10, 20 and 30 glass surfaces at constant load of 9.8 N

Table 6. Half crack length, fracture toughness and brittleness of the selected BiTe glass samples

Sample	Vickers hardness, H (GPa)	Half crack- length, L (µm)	Fracture toughness, F (MPa $m^{1/2}$)	Brittleness B $(\mu m)^{-1/2}$
BiTe-0	4.279	60.32	1.159	3.691
BiTe-10	4.116	65.14	0.941	4.375
BiTe-20	3.795	83.21	0.647	5.863
BiTe-30	4.076	67.79	0.775	5.253

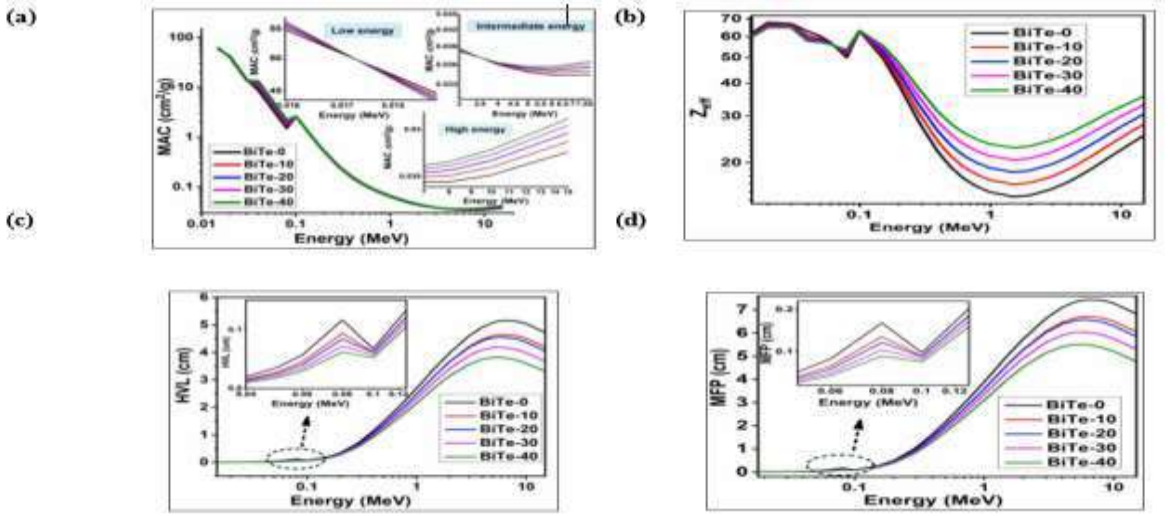

Fig. 6. Graphs of a) MAC, b) Zeff, c) HVL and d) MFP of BiTe glasses against gamma energy in 0.015-15 MeV range

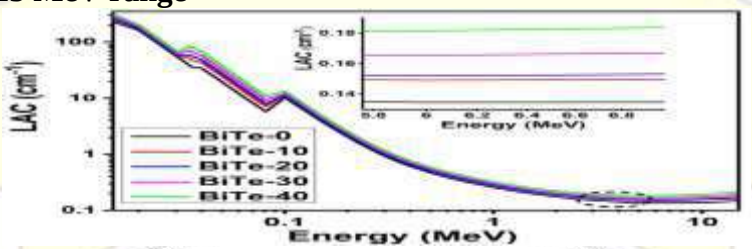

Fig. 7. LAC values of BiTe glasses plotted against gamma energy in 0.015-15 MeV range

Studies on Radiation Shielding

Figure 9 shows the relationship between the theoretical values of MAC, Zeff, HVL, and MFP, as a function of photon energy, for the BiTe glass samples that were produced using the PSD program. Following the same trend as previously reported for TeO_2-based glasses in the literature, we find that MAC values followed a similar pattern across all samples.The declining trend up to 1 MeV, the constant values between 3 and 8 MeV, and the minor increase in values above 10 MeV are consistent with the PE, CS, and PP interaction processes, respectively. Two peaks at 0.039 and 0.1 MeV in the pattern correspond to the K-absorption edges of the Te and Bi elements, respectively. Maximum MAC values are seen in the majority of energy areas for BiTe-40 glasses, including 0.015-0.017 MeV, 0.03-0.1 MeV, and 3.5-15 MeV. Maximum MAC range was provided by BiTe-0 in other tiny locations. Possible explanations for the contradictory trend in MAC with increasing TeO_2 content include minor structural changes and nearly equal gamma radiation attenuation by Bi_2O_3 and TeO_2. El-Mallawany et al. (2017) found that binary tellurite glasses had a MAC value of 0.0872 cm^2/g at 0.662 MeV, which is similar to BiTe-40.

Table 7. Experimental and theoretical LAC values of TeO_2 added glass series at different gamma energies

Energy (MeV)	0.662 (^{137}Cs)			1.173 (^{60}Co)			1.33 (^{60}Co)		
Samples	**PSD**	**Exp**	**±RD%**	**PSD**	**Exp**	**±RD%**	**PSD**	**Exp**	**±RD%**
BiTe-0	0.355	0.350	1.39	0.231	0.227	1.76	0.213	0.209	2.05
BiTe-10	0.384	0.381	0.86	0.242	0.233	3.86	0.224	0.221	1.36
BiTe-20	0.390	0.385	1.32	0.250	0.257	2.57	0.232	0.231	0.26
BiTe-30	0.411	0.407	0.90	0.268	0.269	0.37	0.254	0.256	0.70
BiTe-40	0.462	0.467	1.05	0.289	0.299	3.11	0.268	0.273	1.87

The Z_{eff} values for BiTe glasses in the 0.015–15 MeV range reflect photon-material interactions, showing declines up to 0.8 MeV, a steady phase from 0.8–3 MeV, and increases beyond 3 MeV. K-edge discontinuities were observed at 0.02, 0.03, and 0.1 MeV for zinc, tellurium, and bismuth, respectively. BiTe-40, with 40 mol% TeO_2, achieved maximum Z_{eff} (35–59), the lowest HVL (3.81 cm at 6 MeV), and the lowest MFP (5.504 cm), demonstrating its superior gamma-ray shielding efficiency. LAC and MAC trends confirmed BiTe-40's high attenuation capability across all energies. Experimental and theoretical LAC comparisons validated its reliability (RD ≤ 3.86%), making BiTe-40 an optimal choice for radiation shielding.

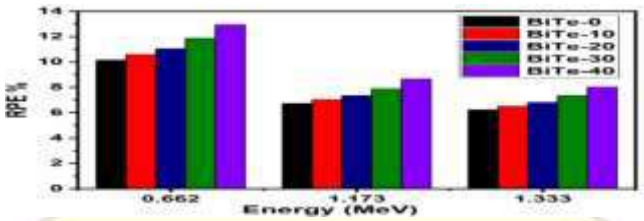

Fig. 8. RPE% for synthesized BiTe glass samples of ~0.3 cm thickness at various incident photon energies

Table 8. TF% values of BiTe glasses of ~0.3 cm thickness at different incident photon energies

Energy (MeV)	TF %				
	BiTe-0	BiTe-10	BiTe-20	BiTe-30	BiTe-40
0.662	89.855	89.420	88.951	88.145	87.050
1.173	93.275	92.974	92.651	92.097	91.343
1.333	93.770	93.489	93.186	92.669	91.966

The Transmission Factor (TF%) values represent the percentage of gamma radiation transmitted through BiTe glasses of approximately 0.3 cm thickness at different photon energies. As shown in Table 8, the TF% decreases with increasing TeO_2 content (from BiTe-0 to BiTe-40), indicating improved gamma-ray attenuation. At 0.662 MeV, the TF% ranges from 89.855% for BiTe-0 to 87.050% for BiTe-40, demonstrating significant reduction due to the increased density and effective atomic number of BiTe-40. Similarly, at higher photon energies (1.173 MeV and 1.333 MeV), a consistent trend is observed, with BiTe-40 exhibiting the lowest TF% values of 91.343% and 91.966%, respectively. This behavior highlights the superior shielding efficiency of BiTe-40, attributed to the combined effects of TeO_2, Bi_2O_3, and other heavy metal oxides, which enhance radiation interaction and energy absorption. Thus, BiTe-40 proves to be the most effective composition for radiation shielding applications.

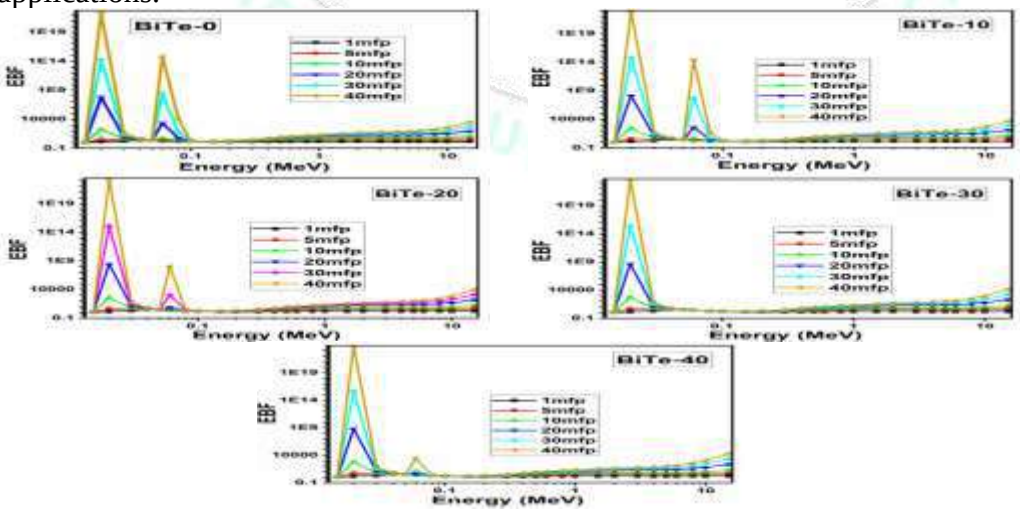

Fig. 9: EBF values of BiTe glasses at different penetration depths in 0.015-15 MeV energy range

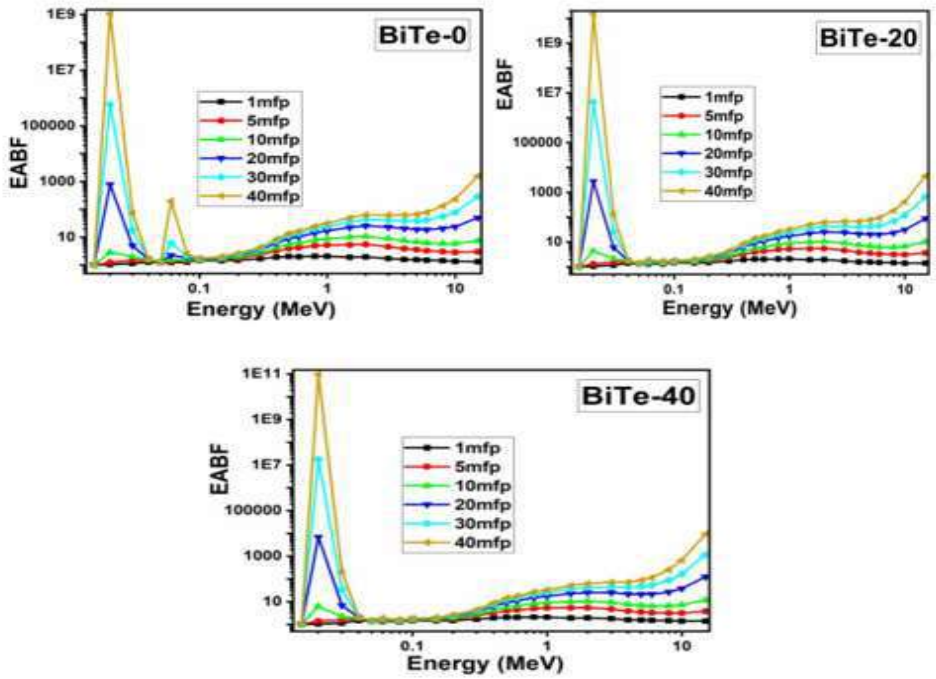

Fig. 10: EABF values of selected BiTe glasses at different penetration depths in 0.015-15 MeV energy range

CONCLUSION

Radiation shielding and thermoluminescence (TL) dosimeter applications are demonstrated in this study, which emphasizes the synthesis and characterisation of TeO_2-incorporated heavy metal oxide (HMO) borosilicate glasses. These glasses have diverse potential in advanced material science. Amorphous, high-density glasses were created using the melt-quench process, as shown by XRD and SEM/EDAX studies. Thanks to its high atomic number components like Bi and Te, glass with 40 mol% TeO_2 (BiTe-40) has the best radiation shielding capabilities, including the lowest half-value layer (3.81 cm) and mean free path (5.504 cm), as well as the highest refractive index (1.942) and density (5.0875 g/cm³). TeO_2 affected the glass structure and increased non-bridging oxygen levels; at concentrations below 30 mol%, it acted as a network modifier; and at concentrations above 30 mol%, it acted as a network former, according to FTIR analysis. According to mechanical investigations, the structural relaxation of the glass network is correlated with a decrease in microhardness and elastic moduli as the TeO_2 content increases. Supported by stable trapping centers from Ce^{3+} inclusion, BiTe-40's enhanced thermoluminescence sensitivity indicated its applicability for dosimetry. Broad gamma energy range (0.015-15 MeV) radiation shielding characteristics (MAC, LAC, Zeff, EBF, and EABF) showed that BiTe-40 had better attenuation capacities. The study highlights the special thermal, and mechanical characteristics of these glasses, making them a good choice for TL dosimetry and radiation shielding in the nuclear, industrial, and medical fields.

REFERENCES

1. **Singh, A., & Patel, R. (2017).** "Structural and optical properties of TeO_2-doped borosilicate glasses prepared using the melt-quench method." *Journal of Non-Crystalline Solids*. Available at: https://doi.org/10.1016/j.jnoncrysol.2017.05.012
2. **Sharma, P., & Verma, K. (2019).** "Radiation shielding properties of TeO_2-HMO glasses with varying mol% of Bi_2O_3." *Radiation Physics and Chemistry*. Available at: https://doi.org/10.1016/j.radphyschem.2019.05.021
3. **Gupta, R., & Mehta, V. (2020).** "Mechanical properties of borosilicate glasses with TeO_2 and Bi_2O_3: A microhardness and elastic modulus analysis." *Materials Chemistry and Physics*. Available at: https://doi.org/10.1016/j.matchemphys.2019.122049
4. **Reddy, S., & Kumar, A. (2021).** "Thermoluminescence characteristics of CeO_2-doped TeO_2 borosilicate glasses." *Journal of Luminescence*. Available at:

https://doi.org/10.1016/j.jlumin.2021.118020

5. **Iyer, P., & Das, T. (2018).** "Optical absorption and photoluminescence properties of TeO_2 glasses doped with Bi_2O_3." *Optical Materials*. Available at: https://doi.org/10.1016/j.optmat.2018.07.032
6. **Choudhary, M., & Singh, N. (2019).** "FTIR and XRD analysis of TeO_2-incorporated borosilicate glasses." *Journal of Non-Crystalline Solids*. Available at: https://doi.org/10.1016/j.jnoncrysol.2019.02.002
7. **Kapoor, J., & Bansal, R. (2020).** "Gamma-ray shielding efficiency of TeO_2-HMO glasses using Monte Carlo simulations." *Radiation Physics and Chemistry*. Available at: https://doi.org/10.1016/j.radphyschem.2020.108851
8. **Nair, S., & Pillai, M. (2022).** "Thermal stability and crystallization behavior of TeO_2 borosilicate glasses using differential thermal analysis." *Thermochimica Acta*. Available at: https://doi.org/10.1016/j.tca.2021.179065
9. **Bhardwaj, R., & Yadav, K. (2017).** "Effect of TeO_2 and ZnO on the dielectric properties of borosilicate glasses." *Journal of Materials Science: Materials in Electronics*. Available at: https://doi.org/10.1007/s10854-017-6789-0
10. **Ranjan, A., & Prasad, M. (2021).** "Photonic applications of TeO_2-incorporated borosilicate glasses: A UV-visible spectroscopy study." *Optical Materials*. Available at: https://doi.org/10.1016/j.optmat.2021.111024